Available online at www.sciencedirect.com
ScienceDirect
Journal of Catalysis 254 (2008) 251–262
JOURNAL OF CATALYSIS
www.elsevier.com/locate/jcat

Iron-catalyzed propylene epoxidation by nitrous oxide: Effect of boron on structure and catalytic behavior of alkali metal ion-modified FeO_x/SBA-15

Sufen Yang, Wenming Zhu, Qinghong Zhang, Ye Wang *

State Key Laboratory of Physical Chemistry of Solid Surfaces and Department of Chemistry, College of Chemistry and Chemical Engineering, Xiamen University, Xiamen 361005, PR China

Received 25 November 2007; revised 22 December 2007; accepted 2 January 2008

Abstract

The presence of boron significantly promoted propylene oxide (PO) formation over chlorine-free K^+-modified FeO_x/SBA-15 catalysts with K/Fe ratios $\geqslant$2.5. Boron also improved the catalytic performances of Rb^+- and Cs^+-modified FeO_x/SBA-15 catalysts, whereas it did not play significant roles over Li^+- and Na^+-modified catalysts. Boron-promoted K^+–FeO_x/SBA-15 exhibited the best catalytic performance for PO formation. Potassium ions could enhance the dispersion of FeO_x clusters, forming active iron sites. The addition of K^+ at a higher content destroyed the ordered mesoporous structure of SBA-15, likely causing the reaggregation of iron species. The modification by boron could keep the ordered mesoporous structure and the high dispersion of iron species, which were beneficial to PO formation. The addition of boron with a proper content also suppressed further conversion of PO by diminishing the acidity and basicity of the catalyst. We propose that the interactions among boron, potassium ions, and iron species play pivotal roles in enhancing PO formation.
© 2008 Elsevier Inc. All rights reserved.

Keywords: Propylene epoxidation; Nitrous oxide; Iron catalyst; Alkali metal ion; Boron

1. Introduction

Propylene oxide (PO) is one of the most important synthetic intermediates in chemical industry. Currently, PO is produced mainly through chlorohydrin and organic hydroperoxide processes; however, these processes produce large amounts of byproducts and are not environmentally benign. The direct epoxidation of propylene using a "green" oxidant has attracted much attention in recent years [1,2]. Although the epoxidation of ethylene by oxygen has been commercialized for several decades using Ag-based catalysts, the epoxidation of propylene by oxygen is not successful. PO selectivity can hardly exceed 60% even at a low propylene conversion over most of the catalysts reported to date for the epoxidation of propylene by oxygen [3–12].

Efficient heterogeneous and homogeneous catalysts such as TS-1 [13] and polyoxometalate [14,15] have been reported for the epoxidation of C_3H_6 using H_2O_2 as an oxidant in the liquid phase. However, the high cost of H_2O_2 and the difficulty in its handling are disadvantageous for the direct use of H_2O_2 for C_3H_6 epoxidation. Many studies have contributed to the in situ production of H_2O_2 from a H_2–O_2 gas mixture for C_3H_6 epoxidation [16–23]. Among the catalysts reported to date, the Au–Ti-based vapor-phase catalyst developed by Hayashi et al. [17] has attracted much attention [18–23]. Propylene conversion of >5% and PO selectivity of >90% could be obtained over a modified Au–Ti-based catalyst [22]. The liquid-phase epoxidation of C_3H_6 by O_2 with methanol as a reductant also proceeded efficiently in the presence of Pd and Ti–Al-MCM-22 catalyst or Pd and peroxo-polyoxometalate catalyst [24–28].

Since the work of Duma and Hönicke [29], several research groups have reported that the catalytic epoxidation of C_3H_6 can proceed with good efficiency using N_2O as an oxidant [30–37]. These studies are based on the idea that N_2O may generate an electrophilic oxygen species on a proper catalyst, which may be suitable for C_3H_6 epoxidation. Actually, many studies have shown that N_2O can be used as an efficient oxidant for the selective oxidation of hydrocarbons such as benzene to phenol [38], propane to propylene [39–41], and methane

* Corresponding author. Fax: +86 592 2183047.
E-mail address: wangye@xmu.edu.cn (Y. Wang).

0021-9517/$ – see front matter © 2008 Elsevier Inc. All rights reserved.
doi:10.1016/j.jcat.2008.01.002

to methanol [42]. Although N_2O is still an expensive oxidant, the chemistry concerning its application in selective oxidation catalysis has attracted much attention [38]. Studies of the epoxidation of C_3H_6 using N_2O have shown that iron-based catalysts are effective and that the modification of catalyst by an alkali metal ion (AMI) is indispensable for PO formation. Whereas other research groups worked mainly with FeO_x/SiO_2 catalysts containing very low Fe content (∼0.1 wt%) [29,30,36,37], we focused on the mesoporous silica (SBA-15 or MCM-41)-supported FeO_x catalysts with a Fe content of ∼1 wt%. The mesoporous silica may allow high and homogeneous dispersion of FeO_x species because of its large surface area and ordered mesoporous channel. In previous studies, we found that KCl was the best modifier of FeO_x/SBA-15 for PO formation, and we obtained PO selectivities of 72% and 50% at C_3H_6 conversions of 4.5% and 10%, respectively, over the KCl-modified FeO_x/SBA-15 catalyst [31,32]. However, the use of other potassium salts, such as potassium acetate, as a modifier resulted in significantly lower PO selectivity [32]. An efficient halogen-free catalyst would be desirable, because halogen in the catalyst might function as a radical promoter in the gas phase and might be lost during the reaction. Moreover, the development of an efficient halogen-free catalyst may provide useful information about other catalyst requirements for high selective PO formation.

To gain more insight into the catalyst requirements for obtaining high PO selectivity and to develop an efficient chlorine-free catalyst, we have aimed to improve the catalytic performance of the chlorine-free AMI-modified FeO_x/SBA-15 catalysts by further modification. In a short communication [43], we disclosed that further modification by boron could significantly enhance the catalytic performance of the chlorine-free K^+–FeO_x/SBA-15 catalysts. This paper reports in detail the effects of boron modification on the structure and catalytic behavior of AMI-modified FeO_x/SBA-15 catalysts.

2. Experimental

2.1. Catalyst preparation

SBA-15 was synthesized by a procedure reported previously [44]. In brief, a homogeneous mixture containing a triblock copolymer ($EO_{20}PO_{70}EO_{20}$) and tetraethyl orthosilicate (TEOS) in hydrochloric acid solution was first stirred at 313 K for 20 h; then the resultant gel was subjected to hydrothermal treatment in an autoclave at 373 K for 24 h. The solid product thus obtained was recovered by filtration followed by washing and drying at 323 K in vacuum. SBA-15 was obtained by calcination at 823 K for 6 h in air to remove the organic template. FeO_x/SBA-15 was prepared by impregnation of the calcined SBA-15 powder with an ethanolic solution of [$Fe(acac)_3$] (acac = acetylacetonate) [32]. After ethanol was removed at 343 K, the obtained powdery sample was further dried at 313 K in vacuum overnight and then subjected to calcination at 823 K in air for 6 h. AMI-modified catalysts (e.g., K^+–FeO_x/SBA-15) were prepared by impregnation of the FeO_x/SBA-15 sample with an aqueous solution of alkali metal acetate (e.g., KAc). The catalysts modified by both AMI and boron were prepared by impregnation of the FeO_x/SBA-15 powder with an aqueous solution of alkali metal acetate together with boric acid (H_3BO_3). After impregnation and drying, the catalysts were calcined at 823 K in air for 6 h. The iron content in all of the catalysts was 1.0 wt% unless specified otherwise.

2.2. Catalytic reaction

The catalytic reactions were carried out using a fixed-bed reactor (10 mm i.d.) operated at atmospheric pressure. The catalyst was pretreated in the reactor with a gas flow containing He (40 mL min^{-1}) and O_2 (10 mL min^{-1}) at 823 K for 30 min, followed by purging with He (60 mL min^{-1}) at the same temperature for another 30 min. After the catalyst was cooled to the reaction temperature (typically 623 K), the reactant gas mixture of C_3H_6 and N_2O diluted with He was introduced into the reactor to start the reaction. The products were analyzed by two online gas chromatographs [32,33]. All of the lines and valves between the exit of the reactor and the gas chromatographs were heated to 393 K, to prevent the condensation of organic products. C_3H_6 conversion was calculated on a carbon basis from the concentrations of the products detected (i.e., PO, acrolein, allyl alcohol, acetone, propionaldehyde, acetaldehyde, CO, and CO_2) and the remaining C_3H_6. PO selectivity was evaluated by the fraction of the amount (in mol) of PO in the total amount (in mol) of all the products detected; the difference in carbon number in each product was considered. The reproducibility of C_3H_6 conversion was within ±0.2%, and that of PO selectivity was within ±2%. Carbon balance also was evaluated and found to be generally better than 90%. C_3H_6 conversion decreased gradually with time on stream, probably due to carbon deposition. Typically, the results after 30 min of reaction are shown and used for discussion, unless stated otherwise.

2.3. Catalyst characterization

X-ray diffraction (XRD) measurements were carried out on a Panalytical X'pert Pro Super X-ray diffractometer with CuK_α radiation (40 kV and 30 mA). N_2 adsorption was carried out at 77 K with a Micromeritics TriStar 3000 surface area and porosimetry analyzer. The sample was pretreated at 573 K in vacuum for 3 h before N_2 adsorption. The surface area was calculated by the BET method, and the pore diameter distribution was evaluated by the BJH method. Transmission electron microscopy (TEM) was performed on a Phillips Analytical FEI Tecnai 30 electron microscope operated at an acceleration voltage of 300 kV. Samples for TEM observations were suspended in ethanol and dispersed ultrasonically. Drops of suspensions were applied on a copper grid coated with carbon.

UV–visible (UV–vis) diffuse reflectance spectra were recorded on a Varian Cary-5000 spectrometer equipped with a diffuse–reflectance accessory. The spectra were collected at 200–800 nm using $BaSO_4$ as a reference. Raman spectroscopy measurements were carried out with a Renishaw UV–vis Raman system 1000R. The UV line at 325 nm from a Kimmon IK3201R-F He–Cd laser was used as the excitation source,

to avoid the influence of fluorescence. X-ray photoelectron spectroscopy (XPS) was measured with a Physical Electronics Quantum 2000 Scanning ESCA Microprobe equipment using monochromatic AlK_α radiation. The binding energy was calibrated using the C1s photoelectron peak at 284.6 eV as a reference. Electron paramagnetic resonance (EPR) measurements were carried out on a Bruker EMX EPR spectrometer at X-band frequency (9.46 GHz). A fixed amount of sample was placed in a quartz tube (3 mm o.d.), which was then set in a quartz Dewar vessel in the EPR cavity. The temperature was set at 100 K throughout the experiment.

H_2 temperature-programmed reduction (H_2-TPR), NH_3 temperature-programmed desorption (NH_3-TPD), and CO_2-TPD were performed using a Micromeritics AutoChem II 2920 instrument connected to a ThermoStar GSD 301 T2 mass spectrometer. Typically, the sample (0.1 or 0.2 g) was first pretreated in a quartz reactor with a gas flow containing O_2 and N_2 at 823 K for 1 h, followed by purging with high-purity N_2. For H_2-TPR, after the sample was cooled to 303 K, an H_2–Ar (5 vol% H_2) mixture was introduced into the reactor, and the temperature was raised to 1173 K at a rate of 10 K min^{-1}. The consumption of H_2 was monitored by a thermal conductivity detector. For NH_3-TPD, the adsorption of NH_3 was performed at 393 K in an NH_3–He mixture (10 vol% NH_3) for 1 h, and the remaining or weakly adsorbed NH_3 was purged by high-purity He. TPD was performed in He flow by raising the temperature to 1000 K at a rate of 10 K min^{-1}. The desorbed NH_3 was detected with the mass spectrometer by monitoring the signal with $m/e = 16$, because the parent peak with $m/e = 17$ possibly could be affected by the desorbed water. For CO_2-TPD, a similar procedure was adopted. The adsorption of CO_2 was carried out at 318 K in a CO_2–He mixture (10% vol CO_2) for 1 h, followed by purging with high-purity He. The signal with $m/e = 44$ was used to monitor the desorbed CO_2 during the TPD with a heating rate of 10 K min^{-1} in He flow.

3. Results

3.1. Effect of boron modification on catalytic behavior

3.1.1. Influence of various additives on the catalytic behavior of chlorine-free K^+–FeO_x/SBA-15 catalyst

Our previous studies found that the chlorine-free K^+–FeO_x/SBA-15 catalyst prepared using KAc or KNO_3 as the precursor of K^+ exhibited markedly lower PO selectivity and lower C_3H_6 conversion than the KCl–FeO_x/SBA-15 catalyst [32]. To increase the catalytic performance of the chlorine-free K^+–FeO_x/SBA-15 catalyst, we investigated the modifying effect of various additives added into the K^+–FeO_x/SBA-15 (K/Fe = 2.5) catalyst prepared using KAc as the precursor of K^+. As shown in Table 1, the K^+–FeO_x/SBA-15 (K/Fe = 2.5) catalyst without further modification provided a C_3H_6 conversion of 3.8% and a PO selectivity of 64% at 623 K. Among the various additives examined, barium, boron, and phosphorus were found to significantly enhance PO selectivity. Particularly, the modification by boron not only improved PO selectivity, but also increased C_3H_6 conversion. C_3H_6 conversion and PO selectivity over the B–K^+–FeO_x/SBA-15 catalyst reached 4.8% and 79%, respectively, which were even better than those over the KCl–FeO_x/SBA-15 catalyst [32]. The conversion of N_2O decreased slightly from 2.7% to 2.5% after modification of the K^+–FeO_x/SBA-15 by boron (B/K = 0.5). The efficiency of N_2O used for the oxidation of C_3H_6 to all of the products (including CO and CO_2) was ~30% over the catalysts both with and without boron modification, but that used for PO formation increased from ~9% to ~15% after the modification by boron.

Table 1
Effect of various additives on catalytic performances of K^+–FeO_x/SBA-15 catalysts[a]

Additive[b]	N_2O conv. (%)	C_3H_6 conv. (%)	Selectivity (%)		
			PO	Other oxygenates[c]	CO_x
None	2.7	3.8	64	14	22
Mg	2.4	3.2	60	29	11
Ba	2.6	3.9	73	14	13
B	2.5	4.8	79	12	9.4
Al	2.3	2.1	11	52	37
Tl	3.1	3.0	49	18	33
La	1.5	1.9	11	75	14
Ce	1.0	1.4	49	44	6.9
Dy	1.0	0.94	63	24	13
Zr	0.7	2.3	49	37	14
S	1.7	1.4	3.9	68	28
P	1.7	2.6	70	15	15

[a] Catalyst: Fe content = 1.0 wt%, K/Fe = 2.5, additive/K = 0.5; reaction conditions: $W = 0.2$ g, $T = 623$ K, $F = 60$ mL min^{-1}, $P(C_3H_6) = 2.53$ kPa, $P(N_2O) = 25.3$ kPa.

[b] The sources of Mg, Ba, Al, Tl, La, Ce, Dy, and Zr were metal nitrates; the sources of B, S, and P were H_3BO_3, $(NH_4)_2SO_4$, and $NH_4H_2PO_4$, respectively.

[c] Other oxygenates include propionaldehyde, acrolein, allyl alcohol, acetone and acetaldehyde.

3.1.2. Effect of boron modification on the catalytic behavior of various AMI-modified FeO_x/SBA-15 catalysts

The catalytic performance of various AMI-modified FeO_x/SBA-15 (AMI/Fe = 2.5) catalysts with and without boron modification is characterized in Table 2. In the absence of an AMI, no PO was formed irrespective of the presence or the absence of boron, suggesting that modification by an AMI was essential to epoxidation. In the absence of boron modification, PO selectivity increased significantly on changing the AMI from Li^+ to Na^+. However, a further change in the AMI from Na^+ to K^+, Rb^+, or Cs^+ decreased both PO selectivity and C_3H_6 conversion. The further modification by boron (B/AMI = 0.5) significantly improved the selectivity to PO and decreased that to CO_x for the K^+–, Rb^+–, and Cs^+–FeO_x/SBA-15 catalysts. The modification by boron also increased C_3H_6 conversion of these catalysts. However, the catalytic performances of the Li^+– and Na^+–FeO_x/SBA-15 catalysts were altered only slightly after the addition of boron. Over the B–K^+–FeO_x/SBA-15, B–Rb^+–FeO_x/SBA-15, and B–Cs^+–FeO_x/SBA-15 catalysts, PO selectivity and C_3H_6 conversion were >70% and >4%, respectively, which were higher than those over the Na^+–FeO_x/SBA-15 catalysts with and without boron modification. These three

Table 2
Effect of boron modification on catalytic performances of FeO_x/SBA-15 catalysts modified by various AMIs[a]

Catalyst[b]	N_2O conv. (%)	C_3H_6 conv. (%)	Selectivity (%)		
			PO	Other oxygenates[c]	CO_x
FeO_x/SBA-15	2.1	1.3	0	50	50
B–FeO_x/SBA-15[d]	2.0	2.3	0	59	41
Li^+–FeO_x/SBA-15	2.9	4.1	16	62	22
B–Li^+–FeO_x/SBA-15	2.7	3.5	16	60	24
Na^+–FeO_x/SBA-15	2.2	4.2	69	18	13
B–Na^+–FeO_x/SBA-15	2.3	4.4	66	21	13
K^+–FeO_x/SBA-15	2.7	3.8	64	14	22
B–K^+–FeO_x/SBA-15	2.5	4.8	79	12	9.4
Rb^+–FeO_x/SBA-15	2.6	2.9	54	13	33
B–Rb^+–FeO_x/SBA-15	2.4	4.2	74	13	13
Cs^+–FeO_x/SBA-15	2.8	2.8	45	18	37
B–Cs^+–FeO_x/SBA-15	2.4	4.4	76	13	11

[a] Reaction conditions: $W = 0.2$ g, $T = 623$ K, $F = 60$ mL min^{-1}, $P(C_3H_6) = 2.53$ kPa, $P(N_2O) = 25.3$ kPa.
[b] Fe content = 1.0 wt%, AMI/Fe = 2.5, B/AMI = 0.5.
[c] Other oxygenates include propionaldehyde, acrolein, allyl alcohol, acetone and acetaldehyde.
[d] B/Fe = 1.25.

boron-modified catalysts were also better for PO formation than the KCl–FeO_x/SBA-15, RbCl–FeO_x/SBA-15, and CsCl–FeO_x/SBA-15 catalysts reported previously [32].

3.1.3. Catalytic performance of K^+–FeO_x/SBA-15 and B–K^+–FeO_x/SBA-15 catalysts with different compositions

Table 3 shows the catalytic performances of the K^+–FeO_x/SBA-15 catalysts with different K/Fe molar ratios in the absence and the presence of boron modification. Without boron modification, C_3H_6 conversion and PO selectivity increased significantly as the K/Fe ratio rose from 0 to 2.5. The sum of the selectivities to CO_x and other organic oxygenates, including propionaldehyde, allyl alcohol, acrolein, acetone, and acetaldehyde, decreased at the same time. However, a further increase in the K/Fe ratio to $\geqslant$5.0 significantly decreased C_3H_6 conversion and PO selectivity, and simultaneously drastically increased the selectivity to CO_x to ~70%. After the modification by boron (B/K = 0.5), the catalyst with the K/Fe ratio of 2.5 still exhibited the highest C_3H_6 conversion and PO selectivity. Nevertheless, C_3H_6 conversion and PO selectivity increased more dramatically for the catalysts with K/Fe ratios $\geqslant$5.0 after boron modification. The CO_x formation over these catalysts was greatly suppressed after boron modification. On the other hand, the addition of boron did not exert significant effects on the catalytic performance of the catalysts with lower K/Fe ratios (0.5 and 1.0).

The effect of B/K ratio on catalytic behavior was investigated for the catalysts with K/Fe ratios of 2.5 and 5.0. In both cases (Figs. 1A and 1B), the increase in B/K ratio to 0.5 increased both C_3H_6 conversion and PO selectivity. The selectivity to CO_x decreased significantly at the same time, further confirming that the modification by boron suppressed the formation of CO_x (especially for the samples with a K/Fe ratio of 5.0). When the B/K ratio exceeded 0.5, C_3H_6 conversion dropped markedly, although the change in PO selectivity was not significant. Thus, the optimum B/K ratio for PO formation was 0.5. In the entire range of B/K ratios investigated (0–2.0), the catalysts with the K/Fe ratio of 2.5 exhibited better catalytic performance than those with a K/Fe ratio of 5.0.

Table 3
Effect of boron modification on catalytic performances of K^+–FeO_x/SBA-15 catalysts with different K/Fe ratios[a]

Catalyst[b]	K/Fe	C_3H_6 conv. (%)	Selectivity (%)		
			PO	Other oxygenates[c]	CO_x
FeO_x/SBA-15	0	1.3	0	50	50
B–FeO_x/SBA-15[d]	0	2.3	0	59	41
K^+–FeO_x/SBA-15	0.5	2.1	0.9	56	43
B–K^+–FeO_x/SBA-15	0.5	2.0	0.7	62	37
K^+–FeO_x/SBA-15	1.0	2.3	47	40	13
B–K^+–FeO_x/SBA-15	1.0	2.5	52	36	12
K^+–FeO_x/SBA-15	2.5	3.8	64	14	22
B–K^+–FeO_x/SBA-15	2.5	4.8	79	12	9.4
K^+–FeO_x/SBA-15	5.0	2.3	20	10	70
B–K^+–FeO_x/SBA-15	5.0	4.0	64	11	25
K^+–FeO_x/SBA-15	7.5	1.8	14	14	72
B–K^+–FeO_x/SBA-15	7.5	3.8	50	18	32
K^+–FeO_x/SBA-15	10	1.1	13	15	72
B–K^+–FeO_x/SBA-15	10	3.6	38	20	42

[a] Reaction conditions: $W = 0.2$ g, $T = 623$ K, $F = 60$ mL min^{-1}, $P(C_3H_6) = 2.53$ kPa, $P(N_2O) = 25.3$ kPa.
[b] Fe content = 1.0 wt%, B/K = 0.5.
[c] Other oxygenates include propionaldehyde, acrolein, allyl alcohol, acetone, and acetaldehyde.
[d] B/Fe = 1.25.

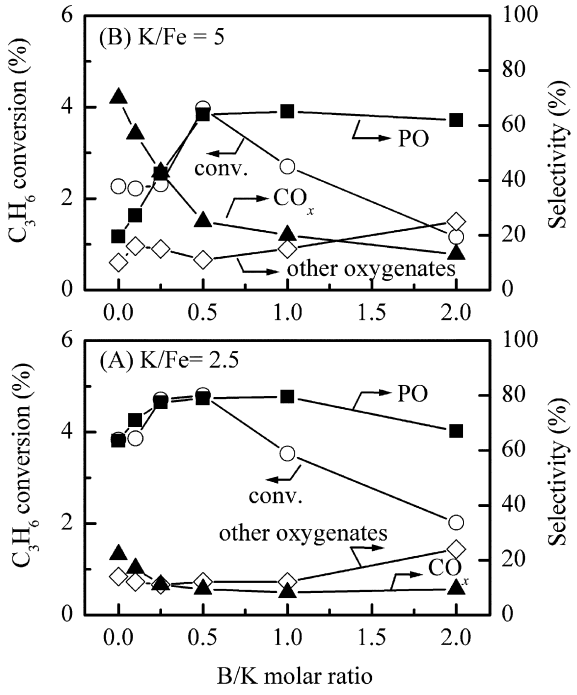

Fig. 1. Effect of B/K ratio on catalytic performances over B–K^+–FeO_x/SBA-15 catalysts with K/Fe ratios of 2.5 (A) and 5.0 (B). Reaction conditions: $W = 0.2$ g, $T = 623$ K, $P(C_3H_6) = 2.53$ kPa, $P(N_2O) = 25.3$ kPa, $F = 60$ mL min^{-1}. Other oxygenates include propionaldehyde, allyl alcohol, acrolein, acetone, and acetaldehyde.

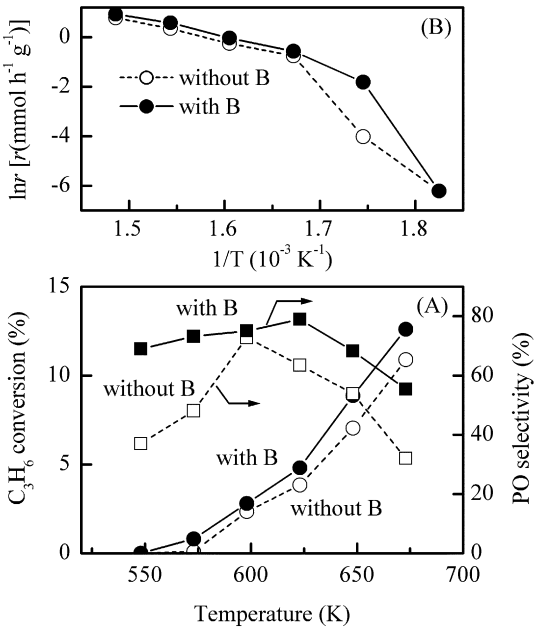

Fig. 2. (A) Temperature dependence of catalytic performances over K^+–FeO_x/SBA-15 (K/Fe = 2.5) and B–K^+–FeO_x/SBA-15 (K/Fe = 2.5, B/K = 0.5) catalysts. Reaction conditions: $W = 0.2$ g, $P(C_3H_6) = 2.53$ kPa, $P(N_2O) = 25.3$ kPa, $F = 60$ mL min^{-1}. (B) Arrhenius plots for conversions of C_3H_6 over K^+–FeO_x/SBA-15 (K/Fe = 2.5) and B–K^+–FeO_x/SBA-15 (K/Fe = 2.5, B/K = 0.5) catalysts.

3.1.4. Comparison of the catalytic behavior of K^+–FeO_x/SBA-15 and B–K^+–FeO_x/SBA-15 catalysts under different reaction conditions

We further compared the catalytic behaviors of the K^+–FeO_x/SBA-15 (K/Fe = 2.5) and B–K^+–FeO_x/SBA-15 (K/Fe = 2.5, B/K = 0.5) catalysts under different reaction conditions. Fig. 2 shows the temperature dependence of catalytic performances. We found that at temperatures ⩽573 K, C_3H_6 conversion was unreasonably lower over both catalysts. For example, C_3H_6 conversion was only ∼0.01% over both catalysts at 548 K, but increased suddenly to 2.3% and 2.8% as the temperature rose to 598 K. This was also reflected in the Arrhenius plots for the two catalysts (Fig. 2B), where the data points at 548 and 573 K ($1/T$, 1.83×10^{-3} and 1.75×10^{-3} K^{-1}) significantly deviated from the straight lines drawn by the higher-temperature data points. Furthermore, PO selectivities were also lower at 548 and 573 K, especially over the catalyst without boron modification. These observations suggest that there exists an "induction temperature" for the epoxidation of C_3H_6 by N_2O over the present catalysts. It is generally accepted that Fe^{II} sites are responsible for the activation of N_2O to form active oxygen species for the selective oxidation of CH_4 or benzene over the $FePO_4$ or Fe-ZSM-5 catalyst [42,45–47]. It is reasonable to speculate that the activation of N_2O also proceeds on the Fe^{II} sites over our catalysts. Thus, the observed "induction temperature" may result from the reduction of the surface iron species by the reactant (i.e., C_3H_6), generating the Fe^{II} sites, for which a relatively higher temperature is needed. The comparison between the two catalysts shown in Fig. 2 reveals that the modification by boron enhanced C_3H_6 conversion at all of the temperatures investigated. The calculation using the straight lines in Fig. 2B ($1/T$, 1.49×10^{-3}–1.67×10^{-3} K^{-1}) provided the same activation energy (i.e., 70 kJ mol^{-1}) for the two catalysts, indicating that the modification by boron may not alter the reaction mechanism. As shown in Fig. 2A, PO selectivity also was improved after the modification by boron at all of the temperatures investigated. Compared with the catalyst without boron modification, the catalyst with boron modification could sustain significantly higher PO selectivity at higher temperatures. For example, over the boron-modified catalyst, PO selectivities of 68% and 55% were obtained at C_3H_6 conversions of 8.9% at 648 K and 13% at 673 K, respectively. These values were significantly higher than those over the catalyst without boron modification (i.e., 54% and 32% at 7.0% and 11% C_3H_6 conversion, respectively). Thus, the further conversion of PO to CO_x at higher reaction temperatures may be suppressed over the catalyst modified by boron.

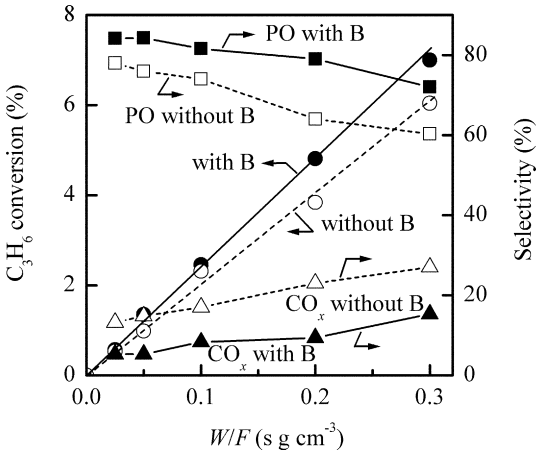

Fig. 3. Dependence of catalytic performances on contact time (W/F) over K^+–FeO_x/SBA-15 (K/Fe = 2.5) and B–K^+–FeO_x/SBA-15 (K/Fe = 2.5, B/K = 0.5) catalysts. Reaction conditions: $T = 623$ K, $P(C_3H_6) = 2.53$ kPa, $P(N_2O) = 25.3$ kPa.

Fig. 3 shows the catalytic behavior of the catalysts with and without boron modification at different contact times, expressed as the ratio of catalyst weight to total flow rate (i.e., W/F). Over both catalysts, C_3H_6 conversion increased almost proportionally to the contact time. From the slope of the straight lines, we calculated the C_3H_6 conversion rate, and found that the modification by boron increased the C_3H_6 conversion rate from 0.81 to 0.98 mmol h^{-1} g^{-1} at 623 K. The selectivity to PO decreased and that to CO_x increased with increasing contact time over both catalysts. However, the selectivity to PO did not approach 100%, and that to CO_x did not approach zero as the contact time approached zero. Thus, we speculate that CO_x may be formed by both consecutive oxidation of PO and direct oxidation of C_3H_6. Comparing the two catalysts demonstrates higher selectivity to PO and lower selectivity to CO_x over the boron-modified catalyst at each contact time. The difference in PO or CO_x selectivity between the two catalysts was greater at longer contact times. Therefore, it is likely that the modification by boron suppresses both the consecutive conversion of PO and the direct oxidation of C_3H_6 to CO_x.

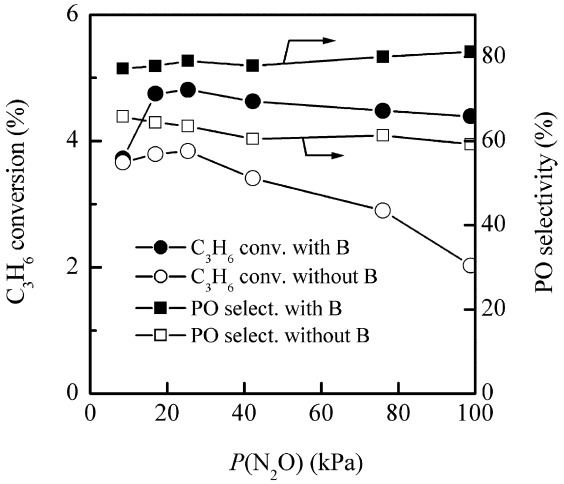

Fig. 4. Effect of partial pressure of N_2O on catalytic performances over K^+–FeO_x/SBA-15 (K/Fe = 2.5) and B–K^+–FeO_x/SBA-15 (K/Fe = 2.5, B/K = 0.5) catalysts. Reaction conditions: $W = 0.2$ g, $T = 623$ K, $P(C_3H_6) = 2.53$ kPa, $F = 60$ mL min^{-1}.

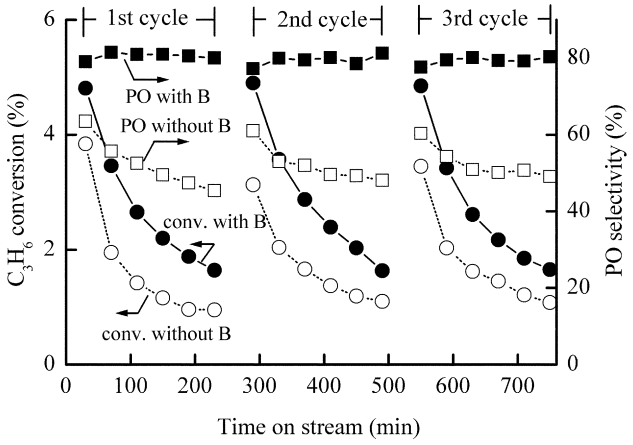

Fig. 5. Changes of catalytic performances with time on stream over K^+–FeO_x/SBA-15 (K/Fe = 2.5) and B–K^+–FeO_x/SBA-15 (K/Fe = 2.5, B/K = 0.5) catalysts. Reaction conditions: $W = 0.2$ g, $P(C_3H_6) = 2.53$ kPa, $P(N_2O) = 25.3$ kPa, $F = 60$ mL min^{-1}. After each cycle, the catalyst was regenerated by a treatment in an O_2-containing gas flow (flow rates of He and O_2, 40 and 10 mL min^{-1}) at 823 K for 30 min following by purge with He flow for 30 min.

We investigated the effect of partial pressure of N_2O [i.e., $P(N_2O)$] on catalytic performance over the two catalysts. As shown in Fig. 4, C_3H_6 conversion increased slightly with increasing $P(N_2O)$ from 8.4 to 25.3 kPa and then decreased over the K^+–FeO_x/SBA-15 catalyst. Over the catalyst with boron modification, C_3H_6 conversion increased with an increase in $P(N_2O)$ from 8.4 to 16.9 kPa, and then remained almost unchanged with a further increase in $P(N_2O)$. PO selectivity did not undergo any significant change with changing $P(N_2O)$ over both catalysts. The catalyst after boron modification exhibited better catalytic performance for PO formation in the entire range of $P(N_2O)$ investigated. Because N_2O is an expensive oxidant, the operation at a lower ratio of N_2O/C_3H_6 is desirable. The results in Fig. 4 also demonstrate that a slight decrease in C_3H_6 conversion occurred when the present catalyst was operated at a relatively lower ratio of N_2O/C_3H_6 (i.e., 3.3).

3.1.5. Stability of K^+–FeO_x/SBA-15 catalysts with and without boron modification

Catalyst deactivation is a common problem over all of the Fe-based catalysts reported for C_3H_6 epoxidation by N_2O [29–37]. The deactivation also has been observed in the epoxidation of C_3H_6 by an O_2–H_2 gas mixture over Au/Ti-based catalysts [21]. We investigated the change of catalytic performances with time on stream over the K^+–FeO_x/SBA-15 (K/Fe = 2.5) and B–K^+–FeO_x/SBA-15 (K/Fe = 2.5, B/K = 0.5) catalysts at 623 K; Fig. 5 shows the results obtained in three cycles of reactions. After each cycle, the catalyst was regenerated by a treatment in an O_2-containing gas flow (at He and O_2 flow rates of 40 and 10 mL min^{-1}, respectively) at 823 K for 30 min, followed by purging with pure He for another 30 min. In each cycle, C_3H_6 conversion and PO selectivity declined with time on stream over the K^+–FeO_x/SBA-15 catalyst. After the modification by boron, PO selectivity remained almost unchanged at ∼80%, although C_3H_6 conversion still decreased with time on stream. Over both catalysts, the catalytic performance could be recovered by the regeneration of catalyst in the O_2-containing gas flow, indicating that carbon deposition was mainly responsible for the catalyst deactivation.

We investigated the effect of adding a small amount of O_2 to the reactant mixture over the B–K^+–FeO_x/SBA-15 (K/Fe = 2.5, B/K = 0.5) catalyst with the aim of removing the carbon deposition and suppressing catalyst deactivation. The stability could be improved gradually by increasing the $P(O_2)$ from 0 to 0.51 kPa (Supplementary material, Fig. S1). Catalyst deactivation was significantly suppressed by co-feeding O_2 with a $P(O_2)$ of 0.17 kPa; however, both C_3H_6 conversion and PO selectivity were decreased due to the presence of O_2. At a $P(O_2)$ of 0.17 kPa, C_3H_6 conversion and PO selectivity remained at ∼2% and ∼50% after 470 min of reaction. The role of co-feeding O_2 in suppressing catalyst deactivation also has been reported in the oxidative dehydrogenation of C_3H_8 by N_2O over iron-containing zeolite catalysts [48].

3.2. Characterizations of K^+–FeO_x/SBA-15 catalysts before and after boron modification

To gain insight into the effect of boron modification on catalyst structures, we focused on characterizing the K^+–FeO_x/SBA-15 series of catalysts with and without boron modification by various techniques.

3.2.1. Ordered mesoporous structure

Fig. 6 shows the XRD patterns at low diffraction angles for the K^+–FeO_x/SBA-15 catalysts with different K/Fe ratios in the absence and the presence of boron modification. The FeO_x/SBA-15 catalyst exhibited three diffraction lines at 2θ degrees of ∼0.9, 1.7, and 1.9°, which were ascribed to the ordered hexagonal arrays of mesoporous structure of SBA-15. Without boron modification (Fig. 6A), the main diffraction peak at 2θ degree of ∼0.9° became significantly weaker as the K/Fe ratio rose to 5.0, and all of the peaks vanished at K/Fe ratios of 7.5 and 10. The surface areas and pore volumes shown in

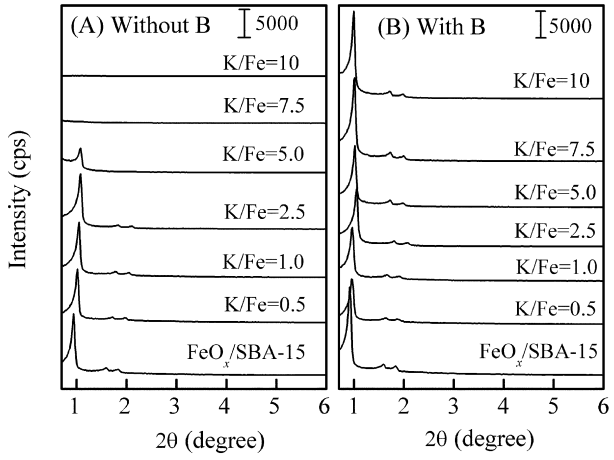

Fig. 6. XRD patterns of K^+–FeO_x/SBA-15 samples with different K/Fe ratios in the absence (A) and the presence (B) of boron (B/K = 0.5).

Table 4
Porous parameters obtained from N_2-physisorption measurements for K^+–FeO_x/SBA-15 samples before and after boron modification (B/K = 0.5)

Sample[a]	K/Fe (molar ratio)	Surface area ($m^2\ g^{-1}$)	Pore volume ($cm^3\ g^{-1}$)	Mean pore diameter (nm)
SBA-15	–	890	1.08	6.4
FeO_x/SBA-15	0	684	0.92	6.3
K^+–FeO_x/SBA-15	0.5	567	0.69	5.4
B–K^+–FeO_x/SBA-15	0.5	597	0.75	5.6
K^+–FeO_x/SBA-15	1.0	476	0.64	5.5
B–K^+–FeO_x/SBA-15	1.0	489	0.67	5.6
K^+–FeO_x/SBA-15	2.5	269	0.52	6.5
B–K^+–FeO_x/SBA-15	2.5	332	0.61	6.6
K^+–FeO_x/SBA-15	5.0	145	0.50	11.5
B–K^+–FeO_x/SBA-15	5.0	294	0.63	7.5
K^+–FeO_x/SBA-15	7.5	61	0.36	24.8
B–K^+–FeO_x/SBA-15	7.5	261	0.56	7.0
K^+–FeO_x/SBA-15	10	54	0.31	24.9
B–K^+–FeO_x/SBA-15	10	231	0.53	7.3

[a] Fe content = 1.0 wt%, B/K = 0.5.

Table 4 underwent significant decreases with increasing K/Fe ratio in the absence of boron. As the K/Fe ratio rose from 2.5 to 5.0 and further to 7.5, the mean pore diameter markedly increased, suggesting the collapse or partial collapse of the mesoporous structure. After the modification by boron (B/K = 0.5), all three diffraction peaks ascribed to the hexagonal regularity of mesoporous structure could be clearly observed for all of the K^+–FeO_x/SBA-15 samples with K/Fe ratios of 0.5–10 (Fig. 6B). The surface areas and pore volumes both increased after the addition of boron; the increases were more significant for the samples with higher K/Fe ratios (5.0–10) (Table 4). After modification by boron, the mean pore diameter for the sample with a K/Fe ratio ⩾5.0 decreased and became close to that for SBA-15.

We further studied the changes in mesoporous structure by TEM. Fig. 7 shows the typical TEM images for the K^+–FeO_x/SBA-15 catalysts before and after boron modification. The ordered mesoporous structure began to collapse due to the unlinking of silica framework as the K/Fe ratio rose to 5.0 (Fig. 7c). The silica framework was completely destroyed at

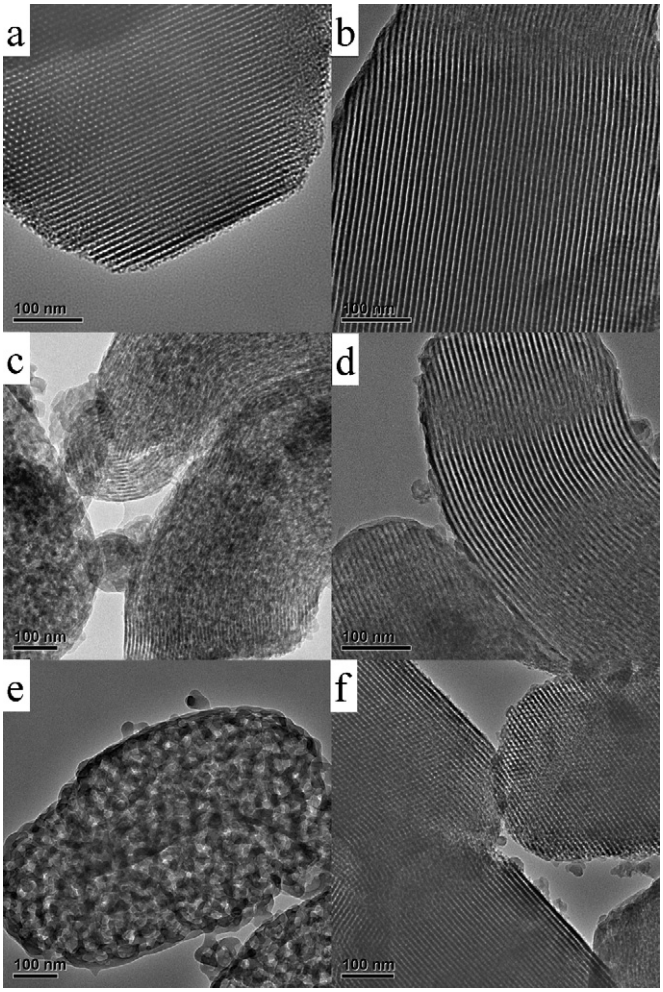

Fig. 7. TEM micrographs. (a), (c), and (e): K^+–FeO_x/SBA-15 with K/Fe ratios of 2.5, 5.0, and 7.5, respectively; (b), (d), and (f): B–K^+–FeO_x/SBA-15 (B/K = 0.5) with K/Fe ratios of 2.5, 5.0, and 7.5, respectively.

a K/Fe ratio of 7.5 in the absence of boron (Fig. 7e). This confirms that the collapse of the ordered mesoporous structure was due mainly to the strong interaction between K^+ and the silica framework. Note that we still could not confirm the formation of FeO_x nanoclusters from the TEM micrographs for the samples with higher K/Fe ratios. After the modification by boron, the well-ordered mesoporous channels could be observed even for the samples with higher K/Fe ratios (i.e., 5.0 and 7.5) (Figs. 7d and 7f). This is in good agreement with the XRD and N_2 adsorption results, confirming that the presence of boron can maintain the ordered mesoporous structure, probably through the interaction between boron species and K^+ ions.

We also studied other alkali metal ion-promoted FeO_x/SBA-15 catalysts in the absence and presence of boron modification. For the Li^+- and Na^+-modified catalysts, the perfect XRD pattern with three diffraction peaks at 2θ degrees of ∼0.9, 1.7, and 1.9° could be sustained even at a Li/Fe or Na/Fe ratio of 5.0. The further modification of these two catalysts by boron did not change the XRD pattern. The surface areas and pore volumes were decreased after boron modification, probably because boron species further occupied the spaces of mesopores. On the other hand, the Rb^+- and Cs^+-modified samples

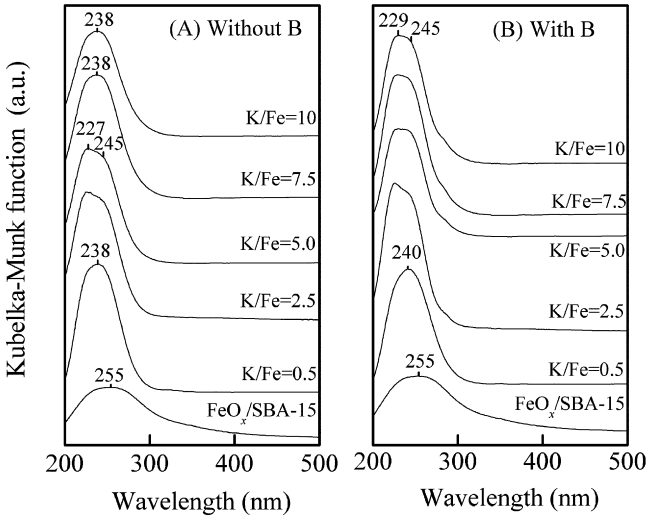

Fig. 8. UV–vis diffuse reflectance spectra of K^+–1 wt% FeO_x/SBA-15 samples with different K/Fe ratios in the absence (A) and the presence (B) of boron (B/K = 0.5).

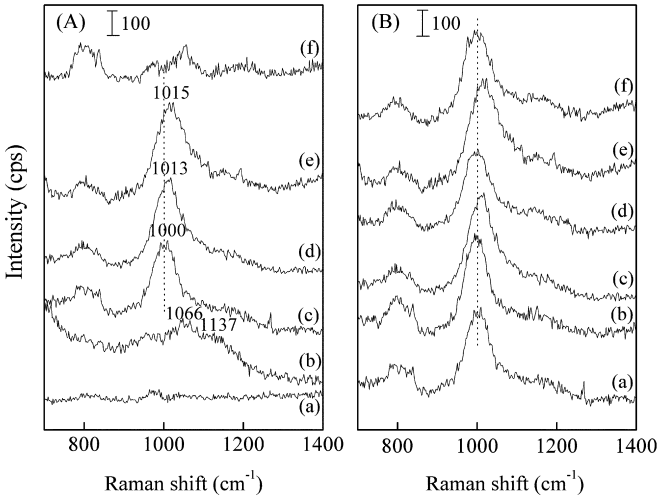

Fig. 9. UV–Raman spectra. (A): (a) SBA-15; (b) FeO_x/SBA-15; (c), (d), and (e) K^+–FeO_x/SBA-15 with K/Fe ratios of 2.5, 7.5, and 10, respectively; (f) K^+–SBA-15 (K/Si = 0.02). (B): (a), (c), and (e) K^+–FeO_x/SBA-15 with K/Fe ratios of 2.5, 7.5, and 10, respectively; (b), (d), and (f) B–K^+–FeO_x/SBA-15 (B/K = 0.5) with K/Fe ratios of 2.5, 7.5, and 10, respectively.

behaved similarly to the K^+-modified FeO_x/SBA-15 samples described above. The increase in the Rb/Fe or Cs/Fe ratio to 5.0 caused the collapse of mesoporous structure in the absence of boron. The presence of boron in these samples could likewise maintain the ordered mesoporous structure.

3.2.2. Structure of iron species

We did not find iron-, potassium-, or boron-related crystalline species from the high-angle XRD patterns for the catalysts used in this work, whereas XRD peaks of crystalline KCl were observed for the KCl–FeO_x/SBA-15 series of catalysts with K/Fe ratios ⩾5.0 [32]. XPS measurements showed that the binding energies of $Fe2p_{3/2}$ were ∼711 eV for the K^+–FeO_x/SBA-15 catalysts with and without boron modification, suggesting that iron was in a Fe(III) state in these samples. The binding energies of B1s were observed at ∼193 eV for the B–K^+–FeO_x/SBA-15 (K/Fe = 2.5) catalysts with B/K ratios of 0.5 to 2.0. This value corresponds to that of boron in the B(III) state.

In previous work [32,33], we clarified that the dispersion of iron species in SBA-15 or MCM-41 could be enhanced by KCl, probably through a surface reaction between KCl and the FeO_x clusters, and we proposed that the tetrahedral iron species thus formed on the surface of SBA-15 was responsible for the epoxidation of C_3H_6 by N_2O. In the present work, we mainly investigated the effect of boron modification on the structure of iron species in K^+–FeO_x/SBA-15 catalysts with different K/Fe ratios. As shown in Fig. 8, the FeO_x/SBA-15 exhibited a broad UV–vis absorption band at 255 nm, which can be assigned to the ligand (O^{2-}) to metal (Fe^{3+}) charge-transfer (LMCT) transition for small FeO_x clusters [32]. The addition of K^+ into the FeO_x/SBA-15 significantly shifted the LMCT transition to a shorter-wavelength position, indicating enhanced dispersion of FeO_x species [32,33,37]. In the absence of boron modification, for the sample with a lower K/Fe ratio (i.e., 0.5), the peak position was observed at 238 nm. As the K/Fe ratio rose to 2.5 and then to 5.0, the absorption pattern changed; two overlapping bands at 227 and 245 nm were observed. It has been reported that the isolated tetrahedral Fe^{3+} site in the framework of MFI zeolite provides two absorption bands at 215 and 241 nm [49]. For the Fe^{3+} (d^5) in tetrahedral coordination with oxygen, the high-spin $e^2t_2^3$ configuration is favored over the $e^4t_2^1$, because the crystal field is not strong enough to cause spin-pairing. This leads to the appearance of two bands ascribed to $t_1 \rightarrow t_2$ and $t_1 \rightarrow e$ transitions [49]. Thus, the two bands observed for our present samples at 227 and 245 nm suggest that iron is in tetrahedral coordination in these samples. This observation is the same with those reported for the KCl–FeO_x/SBA-15 and KCl–FeO_x/MCM-41 samples [32,33]. As the K/Fe ratio rose to 7.5 and then to 10, the absorption pattern changed again and became quite similar to that for the sample with a K/Fe ratio of 0.5, showing a single broad band at 238 nm. This may imply a change in the coordination structure of iron. After the modification by boron (Fig. 8B), the UV–vis spectra for the samples with K/Fe ratios of 0–5.0 did not change significantly. However, for the samples with K/Fe ratios of 7.5 and 10, after the modification by boron, the absorption pattern changed from the single broad band centered at 238 nm to the dual overlapped bands at 227–229 and 245 nm.

UV–Raman spectra for the K^+–FeO_x/SBA-15 samples with and without boron modification are shown in Fig. 9. SBA-15 alone only showed very weak Raman bands at ∼810 and ∼980 cm^{-1} (Fig. 9A, curve a), assignable to the asymmetrical stretching vibrations of ≡Si–OH in the defect sites of SBA-15 [32]. The modification of SBA-15 alone by boron did not change the Raman spectrum significantly. For the FeO_x/SBA-15 (Fig. 9A, curve b), weak and broad bands at 1066 and 1137 cm^{-1} were observed, and these two bands may be ascribed to the finely dispersed FeO_x clusters in SBA-15. The modification of the FeO_x/SBA-15 by K^+ with a K/Fe ratio of 2.5 caused the appearance of a distinct Raman band at 1000 cm^{-1} (Fig. 9A, curve c). This band was not observed

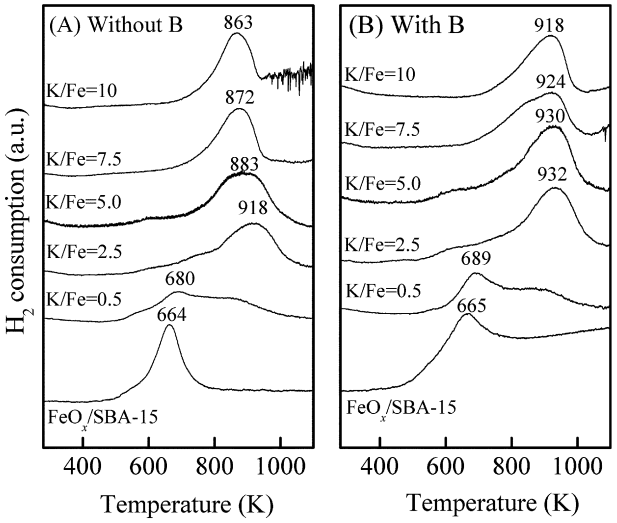

Fig. 10. H_2-TPR profiles of K^+–FeO_x/SBA-15 samples with different K/Fe ratios in the absence (A) and the presence (B) of boron (B/K = 0.5).

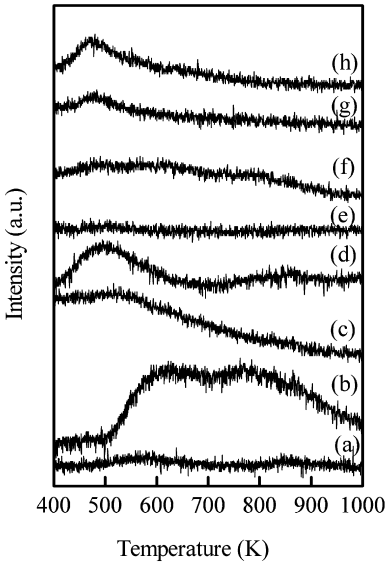

Fig. 11. NH_3-TPD profiles. (a) SBA-15, (b) FeO_x/SBA-15, (c) K^+–FeO_x/SBA-15 (K/Fe = 2.5), (d) K^+–FeO_x/SBA-15 (K/Fe = 5.0), (e) B–K^+–FeO_x/SBA-15 (K/Fe = 2.5, B/K = 0.5), (f) B–K^+–FeO_x/SBA-15 (K/Fe = 5.0, B/K = 0.5), (g) B–K^+–FeO_x/SBA-15 (K/Fe = 2.5, B/K = 2.0), (h) B–K^+–FeO_x/SBA-15 (K/Fe = 5.0, B/K = 2.0).

for the K^+–SBA-15 without iron (Fig. 9A, curve f). The Raman band at 1000 cm^{-1} also was observed for the KCl–FeO_x/SBA-15 catalyst; in previous work, based on a detailed XANES study, we proposed that this band corresponded to the surface tetrahedral iron species [32]. Further increases in K/Fe ratios to 7.5 and 10 in the absence of boron shifted the Raman bands to 1013 and 1015 cm^{-1}, respectively (Fig. 9A, curves d and e). This likely suggests the variation of iron coordination at higher K/Fe ratios. Interestingly, the modification of the samples with K/Fe ratios of 7.5 and 10 by boron (B/K = 0.5) could shift the Raman band again to 1000 cm^{-1} (Fig. 9B, curves d and f). On the other hand, for the sample with a K/Fe ratio of 2.5, the modification by boron did not significantly change the center position of the band at 1000 cm^{-1}.

We also performed EPR studies at 100 K for the K^+–FeO_x/SBA-15 samples in the absence and presence of boron modification. Three signals at $g = 2.0$, 4.3, and 6.0 were observed (Supplementary material, Fig. S2). The assignments of these EPR signals are quite complex [50,51]. The signals at $g = 4.3$ and 6.0 are generally assigned to isolated Fe^{3+} sites in strong rhombic or axial distortion, whereas that at $g = 2.0$ may arise either from isolated Fe^{3+} in high symmetry or from FeO_x clusters [50,51]. In our case, the FeO_x/SBA-15 showed weak and broad signals, possibly due to the strong spin–spin interaction or pairing between Fe^{3+} ions in FeO_x nanoclusters. The intensity of EPR signals increased significantly after modification by K^+, suggesting enhanced dispersion of iron species. The increase in the K/Fe ratio to 5.0 decreased the intensity slightly; however, we found no significant differences between the samples with and without boron modification.

H_2-TPR is also a powerful technique for the characterization of iron structure, because iron species with different structures have different reducibilities [49]. Fig. 10 shows the H_2-TPR profiles for the K^+–FeO_x/SBA-15 samples with and without boron modification. In the temperature region that we investigated, the FeO_x/SBA-15 exhibited a single reduction peak at 664 K, and the quantitative calculation revealed that this peak corresponded to the reduction of Fe^{3+} to Fe^{2+}. The peak shifted significantly to a higher temperature after the addition of K^+ to the FeO_x/SBA-15. It is reported that the reduction of the isolated Fe^{3+} in tetrahedral coordination requires a significantly higher temperature than that of the FeO_x clusters [49,52]. For example, the reduction of Fe^{3+} in the framework of MFI zeolite occurred at >900 K, whereas the reduction of the extra-framework FeO_x species occurred at <700 K [49,52]. Thus, the present H_2-TPR results also indicate enhanced dispersion of Fe species due to the interaction with K^+. The peak temperature increased from 664 to 918 K as the K/Fe ratio rose from 0 to 2.5 (Fig. 10A). However, further increases in K/Fe ratios to 5.0, 7.5, and 10 decreased the peak temperatures to 883, 872, and 863 K, respectively. This likely suggests the reaggregation of iron species to some extent at higher K/Fe ratios. For the FeO_x/SBA-15 without K^+, the modification by boron did not significantly change the peak temperature for the reduction of Fe^{3+} to Fe^{2+} (Fig. 10B). However, for the samples with K^+, the modification by boron (B/K = 0.5) shifted the reduction peak to a higher temperature. Such a shift was more significant at K/Fe ratios ⩾5.0. Therefore, the presence of boron must have increased the dispersion of iron species in the sample modified by K^+ especially with a higher K/Fe ratio.

3.2.3. Acidity and basicity

The modification by K^+ or boron can be expected to affect the acidic and basic properties of catalysts. Fig. 11 shows the NH_3-TPD profiles for SBA-15, FeO_x/SBA-15, K^+–FeO_x/SBA-15, and B–K^+–FeO_x/SBA-15 samples. No desorption of NH_3 was observed over SBA-15 (curve a), in agreement with the fact that SBA-15 does not have acidic sites. Two overlapped NH_3 desorption peaks at ∼630 and ∼770 K were observed over the FeO_x/SBA-15 sample (curve b); these

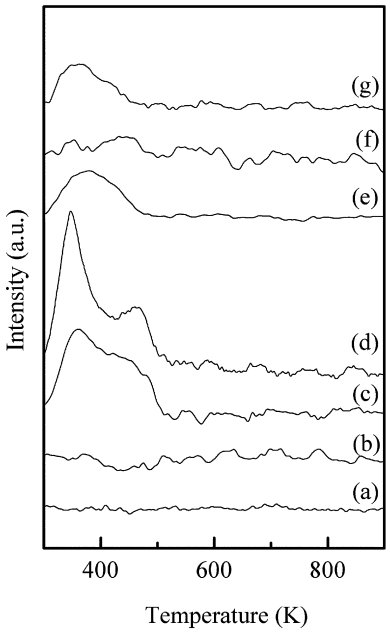

Fig. 12. CO_2-TPD profiles. (a) SBA-15, (b) FeO_x/SBA-15, (c) K^+–FeO_x/SBA-15 (K/Fe = 2.5), (d) K^+–FeO_x/SBA-15 (K/Fe = 5.0), (e) B–K^+–FeO_x/SBA-15 (K/Fe = 2.5, B/K = 0.1), (f) B–K^+–FeO_x/SBA-15 (K/Fe = 2.5, B/K = 0.5), (g) B–K^+–FeO_x/SBA-15 (K/Fe = 5.0, B/K = 0.5).

two peaks were assignable to the desorptions of NH_3 from the Lewis and Brønsted acid sites, respectively [32,53]. We speculate that the Lewis acid sites probably correspond to the FeO_x clusters, whereas the Brønsted acid sites may stem from the disturbed –OH due to the strong interaction of a part of iron with the Si–OH [32]. After modification by K^+, the two peaks almost disappeared (curves c and d). At the same time, a weak peak at ∼500 K was observed, and this peak should arise from weaker Lewis acid sites. This confirms that K^+ ions play significant roles in diminishing catalyst acidity. However, the peak at ∼500 K became stronger as the K/Fe ratio rose from 2.5 to 5.0 (from curves c to d). Thus, K^+ ions also might function as weak Lewis acid sites. It is of interest to note that the further modification by boron with a proper B/K ratio can further weaken catalyst acidity. The peak at ∼500 K ascribed to the weak Lewis acid sites almost vanished for the catalysts with a B/K ratio of 0.5 (curves e and f). This observation also demonstrates the interaction between boron species and K^+ in these catalysts. An increase in the B/K ratio to 2.0 caused the appearance of a new NH_3 desorption peak at ∼475 K (curves g and h), possibly due to the Lewis acid property of the excess boron species.

Fig. 12 shows the CO_2-TPD profiles. SBA-15 and FeO_x/SBA-15 showed no CO_2 desorption peaks below 873 K (curves a and b), suggesting that there were no basic sites on these samples. After the modification of the FeO_x/SBA-15 by K^+ with a K/Fe ratio of 2.5, two CO_2 desorption peaks were observed at 362 and ∼450 K (curve c), indicating the appearance of two types of basic sites. The increase in the K/Fe ratio to 5.0 shifted the two peaks slightly to 348 and 463 K, and the intensity of the lower-temperature peak increased significantly (curve d). The addition of boron into the K^+–FeO_x/SBA-15 (K/Fe = 2.5) markedly changed the CO_2-TPD profile. At a low B/K ratio of 0.1, only one broad peak at ∼378 K was observed (curve e). As the B/K ratio rose to 0.5, almost no CO_2 desorption could be observed over the sample with a K/Fe ratio of 2.5 (curve f). For the sample with a K/Fe ratio of 5.0, a weak and broad CO_2 desorption peak at ∼360 K remained after the modification by boron with a B/K ratio of 0.5 (curve g).

4. Discussion

We found that boron was an efficient promoter for improving the catalytic performance of some halogen-free AMI-modified FeO_x/SBA-15 catalysts for the epoxidation of C_3H_6 by N_2O. The promoting effect of boron was not significant for the Li^+- and Na^+-modified FeO_x/SBA-15 catalysts, but the presence of boron could markedly enhance PO selectivity and C_3H_6 conversion for the K^+-, Rb^+-, and Cs^+-modified catalysts with an AMI/Fe ratio of 2.5 (Table 2). The B- and K^+-doubly promoted catalyst exhibited better catalytic performance for PO formation. For the K^+–FeO_x/SBA-15 series of catalysts, the promoting effect of boron became evident at K/Fe ratios ⩾2.5 (Table 3). Over a B–K^+–FeO_x/SBA-15 catalyst with a K/Fe ratio of 2.5 and a B/K ratio of 0.5, PO selectivities of 79, 68, and 55% could be obtained at C_3H_6 conversions of 4.8% at 623 K, 8.9% at 648 K, and 13% at 673 K. These values exceed those reported previously for the KCl-modified FeO_x/SBA-15 catalyst [32].

Our characterizations using XRD, N_2 physisorption, and TEM clearly revealed that the ordered mesoporous structure of SBA-15 was partially or completely destroyed for the K^+-modified FeO_x/SBA-15 catalysts with K/Fe ratios ⩾5.0. The presence of boron in these catalysts could sustain the ordered mesoporous structure (Figs. 6 and 7). Similar observations were observed for the Rb^+- and Cs^+-modified samples. The results obtained from UV–vis, UV-Raman, and H_2-TPR suggested that the modification of the FeO_x/SBA-15 by K^+ with a proper K/Fe ratio could enhance the dispersion of FeO_x clusters, probably forming tetrahedral Fe^{3+} species on SBA-15. A similar conclusion was also obtained for the KCl–FeO_x/SBA-15 [32] and Rb_2SO_4–FeO_x/SiO_2 [37] catalysts reported previously. In our present work using KAc as a precursor of K^+, the characterizations indicated the occurrence of changes in iron structure accompanying with the collapse of mesoporous structure of SBA-15 at higher K/Fe ratios. The characterization results allow us to speculate that the collapse of the ordered mesoporous structure due to the strong interaction between K^+ and the silica framework of SBA-15 may have caused the reaggregation of iron species attached on the surface of SBA-15. The characterizations also imply that the modification by boron sustained the high dispersion of iron species by maintaining the ordered mesoporous structure even for the catalysts with higher K/Fe ratios. Thus, boron may suppress the strong interaction between K^+ ions and the silica framework and thereby maintain the ordered mesoporous structure and the high dispersion of iron species.

As we reported previously [33], the use of Cab-O-Sil (a nonporous fumed silica) instead of SBA-15 resulted in significantly

Table 5
Catalytic conversion of propylene oxide by N_2O[a]

Catalyst[b]	T (K)	Conv. (%)	Selectivity[c] (%)				
			PA	AA	ACR	AC	CO_x
SBA-15	623	11	34	64	0.6	2.1	Trace
FeO_x/SBA-15	623	100	26	1.8	22	10	22
K^+–FeO_x/SBA-15	623	11	12	9.8	8.1	47	16
	648	39	2.8	3.6	3.7	31	57
	673	72	1.0	1.7	1.9	26	68
B–K^+–FeO_x/SBA-15	623	9.8	12	10	11	45	14
	648	25	7.2	10.4	4.3	35	41
	673	40	4.5	9.8	3.3	26	55

[a] Reaction conditions: $P(PO) = 0.084$ kPa, $P(Ar) = 8.4$ kPa, $P(N_2O) = 25.3$ kPa, He was used as a balance, W(catalyst) $= 0.05$ g, $F = 60$ ml min^{-1}.
[b] Fe content = 1 wt%, K/Fe = 2.5, B/K = 0.5.
[c] PA = propionaldehyde, AA = allyl alcohol, ACR = acrolein, AC = acetone. Others products include acetaldehyde and small amounts of methane, ethane, ethylene and propylene.

lower C_3H_6 conversion and PO selectivity. We believe that the main role of SBA-15 is to maintain the high dispersion of iron species on its surface. The combination of the catalytic results and the structural information described above suggests that the higher dispersion of iron species plays a pivotal role in obtaining both higher PO selectivity and higher C_3H_6 conversion. Analyzing the catalytic performance of all of the catalysts investigated in this work allows us to speculate that K^+, Rb^+, and Cs^+ ions are essentially better modifiers than Na^+ and Li^+ ions for PO formation. It is likely that K^+, Rb^+, and Cs^+ ions interact more effectively with the FeO_x clusters to generate the highly dispersed iron species; however, these ions also may cause partial or complete collapse of the ordered mesoporous structure and reaggregation of iron species, resulting in a significant decrease in PO selectivity and C_3H_6 conversion along with a simultaneous increase in CO_x selectivity. The presence of boron maintains the ordered mesoporous structure and the high dispersion of iron species, thereby enhancing both PO selectivity and C_3H_6 conversion. On the other hand, Li^+ or Na^+ ions with even higher content exerted no significant effect on the ordered mesoporous structure. The further modification of Li^+- or Na^+-promoted catalysts by boron may not affect the dispersion of iron species and thus can not significantly change the catalytic performance.

The present work also revealed that boron exerts significant effects on the acidity and basicity of catalysts. Although the presence of K^+ markedly decreased the acidity due to iron species, weak Lewis acidity remained. The modification by boron with a proper B/K ratio could further diminish such weak Lewis acidity. The basic sites arising from K^+ ions also were decreased by boron modification. Neutralization of the catalyst surface is also believed to contribute to the increased PO selectivity by inhibiting the acid- or base-catalyzed conversions of PO [54]. To clarify this point, we performed catalytic conversion of PO in the presence of N_2O. As shown in Table 5, PO conversion over the FeO_x/SBA-15 was 100% at 623 K. The addition of K^+ into the FeO_x/SBA-15 catalyst (K/Fe = 2.5) markedly decreased the PO conversion. A further modification of the K^+–FeO_x/SBA-15 catalyst by boron (B/K = 0.5) caused a further decrease in PO conversion. Moreover, such a decrease became more significant at a higher temperature. Therefore, boron also should play a significant role in suppressing the consecutive conversion of PO during C_3H_6 epoxidation, probably by diminishing either the acidity or the basicity on catalyst surface. This also can explain the result shown in Fig. 2 that compared with the K^+–FeO_x/SBA-15, the B–K^+–FeO_x/SBA-15 catalyst can sustain a significantly higher PO selectivity at a higher temperature.

Our findings demonstrate that interactions between the boron species and K^+, Rb^+, or Cs^+ ion are crucial for sustaining the ordered mesoporous structure and thereby maintaining a high dispersion of iron species. This interaction also may be the key point for modifying the acidic and basic properties of catalysts. Other acidic modifiers may play similar roles. Actually, phosphorus also enhanced PO selectivity, as shown in Table 1. However, after modification of the K^+–FeO_x/SBA-15 by phosphorus, C_3H_6 conversion decreased. The modification by sulfur, a stronger acidic modifier, significantly decreased both C_3H_6 conversion and PO selectivity (Table 1). Further studies involving changing the P/K or S/K ratio could not improve the catalytic performances (Supplementary material, Table S1). We clarified that the modification by phosphorus could not improve the ordered mesoporous structure of SBA-15, possibly leading to its poorer modifying effect compared with boron. On the other hand, the presence of sulfur did significantly improve the regularity of the ordered mesoporous structure for K^+–FeO_x/SBA-15 (K/Fe = 5.0) (Supplementary material, Fig. S3). High-angle XRD measurements showed the formation of K_2SO_4 crystallites in this case (Supplementary material, Fig. S4), demonstrating a very strong interaction between sulfur and K^+ occurring after the modification by sulfur. This overly strong interaction could have weakened the interaction between K^+ and the iron species, leading to the decreased catalytic performance. In contrast, with boron modification, we found no formation of potassium borate. We speculate that there exist proper interactions among boron, potassium, and iron species that result in high PO formation activity. Moreover, boron might have the capability of improving the electrophilicity of the oxygen species derived from N_2O because of its electron-deficient nature.

5. Conclusion

Boron was found to be an efficient promoter for improving the catalytic performances of halogen-free K^+-, Rb^+-, or Cs^+-modified FeO_x/SBA-15 catalysts for propylene epoxidation by nitrous oxide. The presence of boron significantly enhanced the selectivity to PO and decrease that to CO_x. The modification by boron also increased propylene conversion. For the K^+–FeO_x/SBA-15 series of catalysts, the promoting effect of boron became evident at K/Fe ratios $\geqslant 2.5$. The B- and K^+-doubly promoted catalyst exhibited the best PO formation activity, and PO selectivity of 79% and 68% could be obtained at propylene conversions of 4.8% at 623 K and 8.9% at 648 K. K^+ ions enhanced the dispersion of FeO_x clusters, forming a tetrahedral iron species on the surface of SBA-15 responsible for propylene

epoxidation by nitrous oxide. However, K^+ ions also could react with the silica framework of SBA-15 and lead to the partial or complete collapse of the ordered mesoporous structure. The reaggregation of iron species likely occurred, accompanied by the collapse of the ordered mesoporous structure. The presence of boron could sustain the ordered mesoporous structure and thereby maintain the high dispersion of iron species. The modification by boron also played a significant role in preventing PO from further conversion by neutralizing the catalyst surface. The proper interactions among boron, potassium ion, and iron species are proposed to be crucial in obtaining high PO formation activity.

Acknowledgments

This work was supported by the Natural Science Foundation of China (20625310, 20773099 and 20433030), the National Basic Program of China (2003CB615803 and 2005CB221408), the Key Scientific Project of Fujian Province (2005HZ01-3), and the Program for New Century Excellent Talents at the University of China (NCET-040602, grant to Y.W.).

Supplementary material

The online version of this article contains additional supplementary material.

Please visit DOI: 10.1016/j.jcat.2008.01.002.

References

[1] J.R. Monnier, Appl. Catal. A 221 (2001) 73.
[2] T.A. Nijhuis, M. Makkee, J.A. Moulijn, B.M. Weckhuysen, Ind. Eng. Chem. Res. 45 (2006) 3447.
[3] K. Murata, Y. Kiyozumi, Chem. Commun. (2001) 1356.
[4] B. Cooker, A.M. Gaffney, J.D. Jewson, W.H. Onimus, U.S. Patent 5780657 (1998), to ARCO Chemical Technology, L.P.
[5] G.Z. Lu, X.B. Zuo, Catal. Lett. 58 (1999) 67.
[6] J. Lu, M. Luo, H. Lei, C. Li, J. Catal. 211 (2002) 552.
[7] G.J. Jin, G.Z. Lu, Y.L. Guo, Y. Guo, J.S. Wang, X.H. Liu, Catal. Lett. 87 (2003) 249.
[8] O.P.H. Vaughan, G. Kyriakou, N. Macleod, M. Tikhov, R.M. Lambert, J. Catal. 236 (2005) 401.
[9] J. Lu, J.J. Bravo-Suárez, A. Takahashi, M. Haruta, S.T. Oyama, J. Catal. 232 (2005) 85.
[10] J. Lu, J.J. Bravo-Suárez, M. Haruta, S.T. Oyama, Appl. Catal. A 302 (2006) 283.
[11] N. Mimura, S. Tsubota, K. Murata, K.K. Bando, J.J. Bravo-Suarez, M. Haruta, S.T. Oyama, Catal. Lett. 110 (2006) 47.
[12] H. Chu, L. Yang, Q. Zhang, Y. Wang, J. Catal. 241 (2006) 225.
[13] M.G. Clerici, G. Bellussi, U. Romano, J. Catal. 129 (1991) 159.
[14] Z. Xi, N. Zhou, Y. Su, K. Li, Science 292 (2001) 1139.
[15] K. Kamata, K. Yonehara, Y. Sumida, K. Yamaguchi, S. Hikichi, N. Mizuno, Science 300 (2003) 964.
[16] R. Meiers, U. Dingerdissen, W.F. Hölderich, J. Catal. 176 (1998) 376.
[17] T. Hayashi, K. Tanaka, M. Haruta, J. Catal. 178 (1998) 566.
[18] M. Haruta, Chem. Rec. 3 (2003) 75.
[19] A.K. Sinha, S. Seelan, S. Tsubota, M. Haruta, Top. Catal. 29 (2004) 95.
[20] A.K. Sinha, S. Seelan, S. Tsubota, M. Haruta, Angew. Chem. Int. Ed. 43 (2004) 1546.
[21] A.K. Sinha, S. Seelan, M. Okumura, T. Akita, S. Tsubota, M. Haruta, J. Phys. Chem. B 109 (2005) 3956.
[22] B. Chowdhury, J.J. Bravo-Sárez, M. Daté, S. Tsubota, M. Haruta, Angew. Chem. Int. Ed. 45 (2006) 412.
[23] E. Sacaliu, A.M. Beale, B.M. Weckhuysen, T.A. Nijhuis, J. Catal. 248 (2007) 235.
[24] K. Murata, Y. Liu, N. Mimura, M. Inaba, J. Catal. 220 (2003) 513.
[25] Y. Liu, K. Murata, M. Inaba, N. Mimura, Appl. Catal. A 309 (2006) 91.
[26] Y. Liu, K. Murata, N. Inaba, Chem. Commun. (2004) 582.
[27] Y. Liu, K. Murata, M. Inaba, Green Chem. 6 (2004) 510.
[28] Y. Liu, K. Murata, T. Hanaoka, M. Inaba, K. Sakanishi, J. Catal. 248 (2007) 277.
[29] V. Duma, D. Hönicke, J. Catal. 191 (2000) 93.
[30] E. Ananieva, A. Reitzmann, Chem. Eng. Sci. 59 (2004) 5509.
[31] X. Wang, Q. Zhang, Q. Guo, Y. Lou, L. Yang, Y. Wang, Chem. Commun. (2004) 1996.
[32] X. Wang, Q. Zhang, S. Yang, Y. Wang, J. Phys. Chem. B 109 (2005) 23500.
[33] Q. Zhang, Q. Guo, X. Wang, T. Shishido, Y. Wang, J. Catal. 239 (2006) 105.
[34] A. Costine, T. O'Sullivan, B.K. Hodnett, Catal. Today 112 (2006) 103.
[35] Y. Wang, W. Yang, L. Yang, X. Wang, Q. Zhang, Catal. Today 117 (2006) 156.
[36] T. Thömmes, S. Zürcher, A. Wix, A. Reitzmann, B. Kraushaar-Czarnetzki, Appl. Catal. A 318 (2007) 160.
[37] B. Moens, H.D. Winne, S. Corthals, H. Poelman, R. De Gryse, V. Meynen, P. Cool, B.F. Sels, P.A. Jacobs, J. Catal. 247 (2007) 86.
[38] G.I. Panov, CATTECH 4 (2000) 18.
[39] J. Pérez-Ramírez, E.V. Kondratenko, Chem. Commun. (2003) 2152.
[40] K. Nowińska, A. Waclaw, A. Izbińska, Appl. Catal. A 243 (2003) 225.
[41] R. Bulánek, B. Wichterlová, K. Novoveská, V. Kreibich, Appl. Catal. A 264 (2004) 13.
[42] Y. Wang, K. Otsuka, J. Chem. Soc. Faraday Trans. 91 (1995) 3953.
[43] S. Yang, Q. Zhang, Y. Wang, Chem. Lett. 36 (2007) 786.
[44] D. Zhao, J. Feng, Q. Huo, N. Melosh, G.H. Fredrickson, B.F. Chmelka, G.D. Stucky, Science 279 (1998) 548.
[45] K.A. Dubkov, N.S. Ovanesyan, A.A. Shteinman, E.V. Starokon, G.I. Panov, J. Catal. 207 (2002) 341.
[46] I. Yuranov, D.A. Bulushev, A. Renken, L. Kiwi-Minsker, J. Catal. 227 (2004) 138.
[47] E. Hensen, Q. Zhu, P.-H. Liu, K.-J. Chao, R. van Santen, J. Catal. 226 (2004) 466.
[48] A. Gallardo-Llamas, C. Mirodatos, J. Pérez-Ramírez, Ind. Eng. Chem. Res. 44 (2005) 455.
[49] S. Bordiga, R. Buzzoni, F. Geobaldo, C. Lamberti, E. Giamello, A. Zecchina, G. Leofanti, G. Petrini, G. Tozzola, G. Vlaic, J. Catal. 158 (1996) 486.
[50] A. Ribera, I.W.C.E. Arends, S. de Vries, J. Pérez-Ramírez, R.A. Sheldon, J. Catal. 196 (2000) 287.
[51] M.S. Kumar, M. Schwidder, W. Grünert, A. Brückner, J. Catal. 227 (2004) 384.
[52] J. Pérez-Ramírez, G. Mul, F. Kapteijn, J.A. Moulijn, A.R. Overweg, A. Doménech, A. Ribera, I.W.C.E. Arends, J. Catal. 207 (2002) 113.
[53] Y. Wang, Q. Zhang, T. Shishido, K. Takehira, J. Catal. 209 (2002) 186.
[54] J.M. Coxon, R.G.A.R. Maclagan, A. Rauk, A.J. Thorpe, D. Whalen, J. Am. Chem. Soc. 119 (1997) 4712.